LA-UR -80-1280

TITLE: EFFECT OF THE NUCLEAR EQUATION OF STATE ON HIGH-ENERGY HEAVY-ION COLLISIONS

AUTHOR(S): J. R. Nix, T-9
A. J. Sierk, T-9
D. Strottman, T-9

MASTER

SUBMITTED TO: For presentation at the Seminar on High-Energy Nuclear Interactions and Properties of Dense Nuclear Matter, Hakone, Japan, July 7-11, 1980

University of California

LOS ALAMOS SCIENTIFIC LABORATORY
Post Office Box 1663 Los Alamos, New Mexico 87545
An Affirmative Action/Equal Opportunity Employer

Form No. 836 R3
St. No. 2629
12/78

UNITED STATES
DEPARTMENT OF ENERGY
CONTRACT W-7405-ENG 36

EFFECT OF THE NUCLEAR EQUATION OF STATE ON HIGH-ENERGY HEAVY-ION COLLISIONS

J. R. Nix, A. J. Sierk, and D. Strottman
Theoretical Division, Los Alamos Scientific Laboratory
Los Alamos, New Mexico 87545

ABSTRACT

On the basis of conventional nuclear fluid dynamics, we study in two separate ways the effect of the nuclear equation of state on high-energy heavy-ion collisions. Our equation of state, which sometimes contains a density isomer, has the property that the speed of sound approaches the speed of light in the limit of infinite compression. In the first way, we solve nonrelativistic equations of motion for various values of the nuclear compressibility coefficient for the expansion of spherically symmetric nuclear matter. The matter is initially compressed and excited in head-on collisions of equal targets and projectiles at a laboratory bombarding energy per nucleon of 250 MeV. When the matter expands to a freezeout density, the remaining thermal energy is superimposed in terms of a Maxwell-Boltzmann distribution with appropriate nuclear temperature. The resulting energy distributions for different values of the compressibility coefficient are similar to one another, but they are significantly different from a Maxwell-Boltzmann distribution corresponding to entirely thermal energy and are moderately different

from the energy distribution corresponding to the Siemens-Rasmussen approximation. In the second way, we solve relativistic equations of motion numerically in three spatial dimensions for the reaction $^{20}Ne + ^{238}U$ at a laboratory bombarding energy per nucleon of 393 MeV, both with and without a density isomer. By integrating over the appropriate ranges of impact parameter, we compute the double-differential cross section $d^2\sigma/dE d\Omega$ corresponding both to all impact parameters and to central collisions constituting 15% of the total cross section. To within numerical uncertainties, the results for the various equations of state are very similar to one anotner except for central collisions at laboratory angle $\theta = 30^\circ$ and for both central collisions and all impact parameters at $\theta = 150^\circ$. In these cases, over certain ranges of energy, $d^2\sigma/dE d\Omega$ is larger for the density isomer than for conventional equations of state.

I. INTRODUCTION

High-energy heavy-ion collisions provide a unique opportunity to explore what happens when heavy nuclei become highly compressed and excited. As part of the recent surge of interest in this area, several calculations of high-energy heavy-ion collisions have been performed on the basis of nuclear fluid dynamics,[1-10] where the fundamental input is the nuclear equation of state. It is of crucial importance to know the sensitivity of the calculated results to the input equation of state.

Although some two-dimensional and three-dimensional calculations have been performed for different equations of state,[5-8] the fairly large numerical errors that are present have precluded an accurate assessment of this sensitivity. We therefore attack this problem in two separate ways. In the first way, we perform a simple one-dimensional nonrelativisitc calculation for which an accurate numerical solution is possible, studying the sensitivity of the energy distribution of expanding spherically symmetric nuclear matter to the nuclear compressibility coefficient. In the second way, we solve the equations of relativistic nuclear fluid dynamics numerically in three spatial dimensions by use of a particle-in-cell finite-difference computing method,[2] both with and without a density isomer. We use an improved treatment of exterior cells that does not require setting their rest-frame density equal to normal nuclear density.

All of our considerations are based on conventional nuclear fluid dynamics, which neglects any interpenetration that the target and projectile may experience upon contact. Although this interpenetration can be taken into account by means of two-fluid dynamics,[11] in which coupled relativistic equations of motion are solved for separate target and projectile nuclear fluids, the effect of the equation of state in such a model has not been explored.

II. NUCLEAR EQUATION OF STATE

The nuclear equation of state, which specifies how the pressure depends upon density and thermal energy, can be written as the sum of a contribution from the compressional energy and a contribution from the thermal energy. This is seen most clearly by recalling that the total internal energy per nucleon is given by[4]

$$E(n,I) = E_0(n) + I \quad ,$$

where $E_0(n)$ is the ground-state energy per nucleon at nucleon number density n and I is the thermal energy per nucleon. The pressure p is then obtained from the fundamental relation[4]

$$p = n^2 \left.\frac{\partial E(n,I)}{\partial n}\right|_S = n^2 \frac{dE_0(n)}{dn} + n^2 \left.\frac{\partial I}{\partial n}\right|_S \quad ,$$

with differentiation at constant entropy per nucleon S.

For the ground-state energy per nucleon $E_0(n)$ we use a new functional form which has the property that the speed of sound approaches the speed of light in the limit of infinite compression. This is achieved by taking $E_0(n)$ for n greater than one or more critical values to be a parabola in the square root of the density, so that in the limit of infinite compression it increases linearly with density. The value of $E_0(n)$ at normal nuclear density n_0 is taken to be -8 MeV to simulate the effects of surface and Coulomb energies for finite nuclei. In the limit of zero density, $E_0(n)$ is taken to be the difference between a specified term proportional to $n^{2/3}$ that represents the kinetic energy of noninteracting nucleons and a term proportional to n whose coefficient is adjusted so that the two forms join smoothly with continuous value and first derivative.

For the case in which there is no density isomer, the resulting ground-state energy $E_0(n)$ is shown in Fig. 1 for five values of the nuclear compressibility coefficient K ranging from 0 to 400 MeV. The curves for K = 200 and 400 MeV are shown again in Fig. 2, where we expand the vertical scale to show more clearly the density isomer in the dot-dashed curve. The isomer is taken to occur at a density that is three times normal nuclear density, with an energy 2 MeV higher than that at normal density and with the same curvature.

For the thermal contribution to the pressure we use the nonrelativistic Fermi-gas model, which yields[4]

$$P_{\text{thermal}} = n^2 \left.\frac{\partial I}{\partial n}\right|_S = \frac{2}{3} n I \quad .$$

Unlike what is often implied, this is a general result for the nonrelativistic Fermi-gas model that is valid to all orders in the temperature.

III. NONRELATIVISTIC SPHERICALLY SYMMETRIC EXPANSION

A. Fluid-dynamical stage

We consider in this section the head-on collision of an equal target and projectile with laboratory bombarding energy per nucleon of 250 MeV, which corresponds relativistically to a center-of-mass energy per nucleon of 60.53 MeV. We make the drastic geometrical assumption that during the collision the nuclear matter is uniformly compressed and excited into a sphere at rest in the center-of-mass system, with initial values of the density, compressional energy, and thermal energy determined by relativistic Rankine-Hugoniot relations.[4] These relations are obtained by integrating the relativistic equations of fluid dynamics over an infinitesimal volume near the contact point in a head-on collision. The solutions for the cases considered here are illustrated in Fig. 1. With increasing compressibility coefficient, the initial

compressional energy per nucleon increases, whereas the initial density and thermal energy per nucleon decrease.

These quantities serve as initial conditions for the spherically symmetric expansion of the matter, which is treated nonrelativistically in two stages. In the first stage, corresponding to densities greater than a freeze-out density,[12-14] we integrate numerically in one dimension nonrelativistic equations of fluid dynamics.[15] Relativistic effects are negligible for the 60.53-MeV center-of-mass initial energy per nucleon considered here. These equations express the conservation of nucleon number, momentum, and energy, for a particular nuclear equation of state. We neglect the surface energy, Coulomb energy, nuclear viscosity, thermal conductivity, and single-particle effects, as well as the production of additional particles and the associated radiative loss of energy from the system.

To integrate the equations of motion we use a Lagrangian technique, with the radial coordinate r divided into 200 points that are initially equally spaced but that move as the matter expands. The time step is taken to be about $3 \cdot 10^{-23}$ s for nonzero values of the compressibility coefficient and about $1 \cdot 10^{-23}$ s for zero compressibility coefficient, corresponding to a perfect gas.

The essential features of the solution are illustrated in Fig. 3 for a compressibility coefficient equal to 200 MeV. For small values of time, the radial expansion of the matter near the surface is accompanied by a rarefaction wave that propagates inwards through the matter that is initially unaffected. This is similar to the one-dimensional expansion of a semi-infinite compressed perfect gas, for which an analytic solution is possible.[15] However, it is to be contrasted with the analytic solution obtained by Bondorf et al.,[16] where the density profile remains rectangular in shape, with a

constant decrease in value and expansion of radius. The reason for this is that in the calculations of Bondorf et al.[16] the interior thermal energy is not constant but is instead assumed to decrease parabolically with increasing radial distance. For larger values of time, our calculated density profile develops a shallow minimum at the center of the nucleus.

The fluid-dynamical calculation is continued until the fluid reaches a freezeout density,[12-14] which is taken to be the point at which either the total pressure becomes zero or the compressional contribution to the pressure reaches its maximum negative value. For our equation of state, the latter criterion occurs at a nucleon number density n that is 9/16 of the equilibrium density n_0. With our initial conditions, this criterion governs the freezeout for K = 100 and 200 MeV. However, for K = 400 MeV, freezeout occurs when $n = 0.75\ n_0$ because the total pressure becomes zero at that point.

As shown in Fig. 4, the resulting energy distribution of the expanding matter at freezeout depends slightly upon the compressibility coefficient. In particular, with increasing compressibility coefficient, the energy distribution becomes slightly higher and narrower. The discontinuities in slope at the high-energy portions of the spectra arise from numerical inaccuracies in the treatment of the outermost cell.

B. Thermal folding

At the freezeout point,[12-14] the expanding matter still contains some thermal energy that contributes to the final energy distribution. To simulate the approximately 8-MeV loss in binding energy per nucleon corresponding to breakup into neutrons and protons rather than composite particles, we measure the remaining thermal energy relative to zero energy rather than relative to the minimum energy at saturation density. This thermal energy is then superimposed in terms of a nonrelativistic Maxwell-Boltzmann distribution, with

temperature equal to 2/3 of the thermal energy per nucleon.

After thermal folding, the energy distributions corresponding to K = 100, 200, and 400 MeV are indistinguishable from one another to within graphical accuracy, as shown by the solid curve in Fig. 5. However, this common result for nonzero compressibility coefficient peaks at a slightly lower energy and has a longer tail than the dashed curve calculated for zero compressibility coefficient, corresponding to the fluid-dynamical expansion of a perfect gas. In order that the average energy per nucleon is the same, this result for K = 0 is calculated for initial conditions corresponding to an energy per nucleon of 52.53 MeV, which is 8 MeV less than the amount illustrated in Fig. 1. Upon comparing with Fig. 4, we see that prior to thermal folding, the energy distributions for nonzero compressibility coefficient are significantly higher and narrower than the distribution for K = 0. However, after thermal folding, the results for zero and nonzero compressibility coefficient are only slightly different from each other.

As shown by the dotted line in Fig. 5, the Maxwell-Boltzmann distribution corresponding to entirely thermal energy, which is used in fireball and fire-streak models,[14,17,18] peaks at a significantly lower energy and has a longer tail than our calculated solid curve. Finally, the dot-dashed curve in Fig. 5 is calculated with the Siemens-Rasmussen approximation,[19] which assumes that one-half the initial energy per nucleon appears as constant kinetic energy, with the other half superimposed in terms of a Maxwell-Boltzmann distribution with appropriate nuclear temperature. Although this result is shifted from the pure Maxwell-Boltzmann curve in the correct direction, it still peaks at a lower energy and has a longer tail than our calculated solid curve.

IV. RELATIVISTIC THREE-DIMENSIONAL SOLUTION

A. Particle-in-cell computational technique

For a given nuclear equation of state and given initial conditions, we solve the equations of relativistic nuclear fluid dynamics numerically in three spatial dimensions by use of a particle-in-cell finite-difference computing method.[2] This technique is applicable to supersonic flow and combines some of the advantages of both Eulerian and Lagrangian methods. To facilitate comparisons with experimental results, the calculations are performed in the laboratory reference frame.

As in previous calculations with this technique, the computational mesh consists of fixed cubical Eulerian cells approximately 1.2 fm in length. The fluid, which moves through this mesh, is represented by about 26,000 discrete Lagrangian particles, corresponding to $3^3 = 27$ particles per cell for nuclear matter at equilibrium density. This is about three times the number of computational particles used previously.

Another improvement in the present calculation concerns our treatment of exterior cells, where the volume occupied by the fluid is in general less than the volume of the cell. In previous calculations, the rest-frame density of all exterior cells was simply set equal to equilibrium nuclear density.[2] Although this procedure is adequate during the early stages of the collision, it becomes increasingly worse during the later expansion stage. We therefore determine the rest-frame density of edge cells by averaging the rest-frame densitites of adjacent interior cells. For exterior cells that are not adjacent to interior cells, we compute the density by assuming that the entire cell volume is occupied by fluid.

B. Cross section $d^2\sigma/dE d\Omega$ for outgoing charged particles

We consider the reaction $^{20}Ne + ^{236}U$ at a laboratory bombarding energy per nucleon of 393 MeV, for which there exist experimental data on the cross section $d^2\sigma/dE d\Omega$ for outgoing charged particles.[20] For each of the three equations of state illustrated in Fig. 2, we solve the equations of motion for five different impact parameters. We continue calculating the fluid-dynamical expansion to relatively small densities, where the thermal energy per nucleon is negligible, rather than perform a thermal folding after freezeout as we did for the spherically symmetric expansion.

By integrating over the appropriate ranges of impact parameter, we compute the double-differential cross section corresponding both to all impact parameters and to central collisions constituting 15% of the total cross section. The cross section for the outgoing matter distribution is then converted into the cross section $d^2\sigma/dE d\Omega$ for outgoing charged particles under the assumption of uniform charge density.

The results calculated for a conventional nuclear equation of state with compressibility coefficient K = 200 MeV are shown in Fig. 6 in the form of energy spectra at four laboratory angles ranging from 30° to 150°. Some measure of the numerical inaccuracies inherent in the calculations can be determined from the fluctuations in the histograms, which are obtained using angular bins of 10° width.

The results calculated for all impact parameters, given in the left-hand side of Fig. 6, are compared with the experimental data of Sandoval et al.[20] for outgoing charged particles, which include contributions from protons, deuterons, tritons, ^3He particles, and ^4He particles. Because of our neglect of binding, at low energy the calculated results at all angles are higher than the experimental results. At higher energy the calculations reproduce, to

within numerical uncertainties, the experimental data at all angles except 150°, where the calculated results are somewhat below the experimental results.

The results calculated for central collisions constituting 15% of the total cross section are given in the right-hand side of Fig. 6. At low energy and all angles these results are significantly below those for all impact parameters. At laboratory angle $\theta = 30°$ the result for central collisions decreases much more rapidly with increasing energy than the result for all impact parameters. However, at $\theta = 150°$ the result for central collisions is at higher energy very similar to that for all impact parameters. We are unable to compare our calculations for central collisions with experimental data because the data for central collisions do not yet include contributions from composite particles but instead include only protons.[21]

As shown in Fig. 7, the results calculated for a conventional nuclear equation of state with K = 400 MeV are very similar, to within numerical uncertainties, to those calculated with K = 200 MeV. Varying the compressibility coefficient alone in a conventional equation of state has little effect on the single-particle-inclusive cross section $d^2\sigma/dE d\Omega$ for either all impact parameters or central collisions.

We show finally in Fig. 8 the results calculated for our equation of state with a density isomer. At most energies and angles these results are very similar, to within numerical uncertainties, to those calculated for conventional equations of state. However, for central collisions at $\theta = 30°$ the results calculated for a density isomer decrease more slowly with increasing energy than those calculated for conventional equations of state. Also, for both central collisions and all impact parameters at $\theta = 150°$ the results calculated for the density isomer are higher than those calculated for

conventional equations of state. These differences arise because at this bombarding energy the softer density-isomer equation of state leads to higher initial density and thermal energy per nucleon, which increases the thermal contribution to the cross section in regions where it would otherwise be small.

V. OUTLOOK

On the basis of conventional nuclear fluid dynamics, both in one dimension for the spherically symmetric expansion of nuclear matter and in three dimensions for the single-particle-inclusive cross section $d^2\sigma/dE d\Omega$ for all impact parameters and for central collisions, we have shown that the calculated results depend very little on the nuclear compressibility coefficient. Thermal folding after freezeout reduces the small differences that are present even further.

A strong density isomer increases the cross section $d^2\sigma/dE d\Omega$ for central collisions at $\theta = 30°$ and for both central collisions and all impact parameters at $\theta = 150°$, but numerical uncertainties are comparable to the effect. Furthermore, the inclusion of transparancy in a more realistic model that goes beyond conventional nuclear fluid dynamics would also increase $d^2\sigma/dE d\Omega$ for central collisions at $\theta = 30°$, which complicates the interpretation of experimental data.

Although current experimental data on relativistic heavy-ion collisions can be understood on the basis of conventional ideas, the work done thus far provides a necessary background for the identification of any new phenomena that may result from high compression and excitation of nuclear matter. Possible directions for the future include studies of excitation functions, two-particle correlations, impact-parameter dependences, particle-multiplicity

distributions, the deuteron/proton ratio, and the Coulomb distortion of charged-pion spectra.

We are grateful to J. I. Kapusta and J. W. Negele for stimulating discussions. This work was supported by the U. S. Department of Energy.

REFERENCES

1. A. A. Amsden, G. F. Bertsch, F. H. Harlow, and J. R. Nix, Phys. Rev. Lett. 35, 905 (1975).
2. F. H. Harlow, A A. Amsden, and J. R. Nix, J. Comp. Phys. 20, 119 (1976).
3. A. A. Amsden, F. H. Harlow, and J. R. Nix, Phys. Rev. C 15, 2059 (1977).
4. J. R. Nix, Prog. Part. Nucl. Phys. 2, 237 (1979).
5. H. Stöcker, J. A. Maruhn, and W. Greiner, Z. Phys. A290, 297 (1979).
6. H. Stöcker, J. A. Maruhn, and W. Greiner, Z. Phys. A293, 173 (1979).
7. H. Stöcker, R. Y Cusson, J. A. Maruhn, and W. Greiner, Z. Phys. A294, 125 (1980).
8. P. Danielewicz, Nucl. Phys. A314, 465 (1979).
9. L. P. Csernai, H. W. Barz, B. Lukács, and J. Zimányi, in Proceedings of the EPS Topical Conference on Large Amplitude Collective Nuclear Motions, Keszthely, Hungary, 1979 (Central Research Institute for Physics, Budapest, 1979), Vol. II, p. 533.
10. H. H. K. Tang and C. Y. Wong, Phys. Rev. C, to be published.
11. A. A. Amsden, A. S. Goldhaber, F. H. Harlow, and J. R. Nix, Phys. Rev. C 17, 2080 (1978).
12. A. Mekjian, Phys. Rev. Lett. 38, 640 (1977).
13. R. Bond, P. J. Johansen, S. E. Koonin, and S. Garpman, Phys. Lett. 71B, 43 (1977).
14. J. I. Kapusta, Phys. Rev. C 16, 1493 (1977).

15. F. H. Harlow and A. A. Amsden, Los Alamos Scientific Laboratory Report No. LA-4700 (1971).

16. J. P. Bondorf, S. I. A. Garpman, and J. Zimányi, Nucl. Phys. A296, 320 (1978).

17. G. D. Westfall, J. Gosset, P. J. Johansen, A. M. Poskanzer, W. G. Meyer, H. H. Gutbrod, A. Sandoval, and R. Stock, Phys. Rev. Lett. 37, 1202 (1976).

18. W. D. Myers, Nucl. Phys. A296, 177 (1978).

19. P. J. Siemens and J. O. Rasmussen, Phys. Rev. Lett. 42, 880 (1979).

20. A. Sandoval, H. H. Gutbrod, W. G. Meyer, R. Stock, C. Lukner, A. M. Poskanzer, J. Gosset, J. C. Jourdain, C. H. King, G. King, V. S. Nguyen, G. D. Westfall, and K. L. Wolf, Phys. Rev. C 21, 1321 (1980).

21. R. Stock, H. H. Gutbrod, W. G. Meyer, A. M. Poskanzer, A. Sandoval, J. Gosset, C. H. King, C. Lukner, V. S. Nguyen, G. D. Westfall, and K. L. Wolf, Gesellschaft für Schwerionenforschung Preprint No. GSI-Preprint-79-22 (1979).

FIGURE CAPTIONS

Fig. 1. Compressional contribution to our conventional nuclear equation of state, for five values of the compressibility coefficient K. The arrows denote the thermal energy per nucleon I and the nucleon number density n achieved in the head-on collision of an equal target and projectile with laboratory bombarding energy per nucleon of 250 MeV.

Fig. 2. Compressional contribution to our conventional nuclear equation of state, for two values of the compressibility coefficient K, and to our equation of state with a density isomer.

Fig. 3. Time evolution of the density profile for the spherically symmetric expansion of matter that is initially compressed and excited in the head-on collision of an equal target and projectile with a laboratory bombarding energy per nucleon of 250 MeV. The nuclear compressibility coefficient K is 200 MeV.

Fig. 4. Distribution of kinetic energy per nucleon at the freezeout point, for three values of the nuclear compressibility coefficient K, and for the expansion of a perfect gas that is initially compressed and excited with a center-of-mass energy per nucleon of 52.53 MeV.

Fig. 5. Distribution of kinetic energy per nucleon after superimposing the thermal energy at freezeout in terms of a nonrelativisitc Maxwell-Boltzmann distribution. The results for three values of the nuclear compressibility coefficient K are indistinguishable from one another to within graphical accuracy and are shown by the solid curve, which is compared to three other distributions with the same average energy per nucleon.

Fig. 6. Charged-particle energy spectrum $d^2\sigma/dE d\Omega$ calculated for our conventional nuclear equation of state with compressibility coefficient K = 200 MeV. The histograms calculated for all impact parameters are compared in the left-hand side of the figure with the experimental data of Sandoval et al.[20]

Fig. 7. Charged-particle energy spectrum $d^2\sigma/dE d\Omega$ calculated for our conventional nuclear equation of state with compressibility coefficient K = 400 MeV. The histograms calculated for all impact parameters are compared in the left-hand side of the figure with the experimental data of Sandoval et al.[20]

Fig. 8. Charged-particle energy spectrum $d^2\sigma/dE d\Omega$ calculated for our nuclear equation of state with a density isomer. The histograms calculated for all impact parameters are compared in the left-hand side of the figure with the experimental data of Sandoval et al.[20]

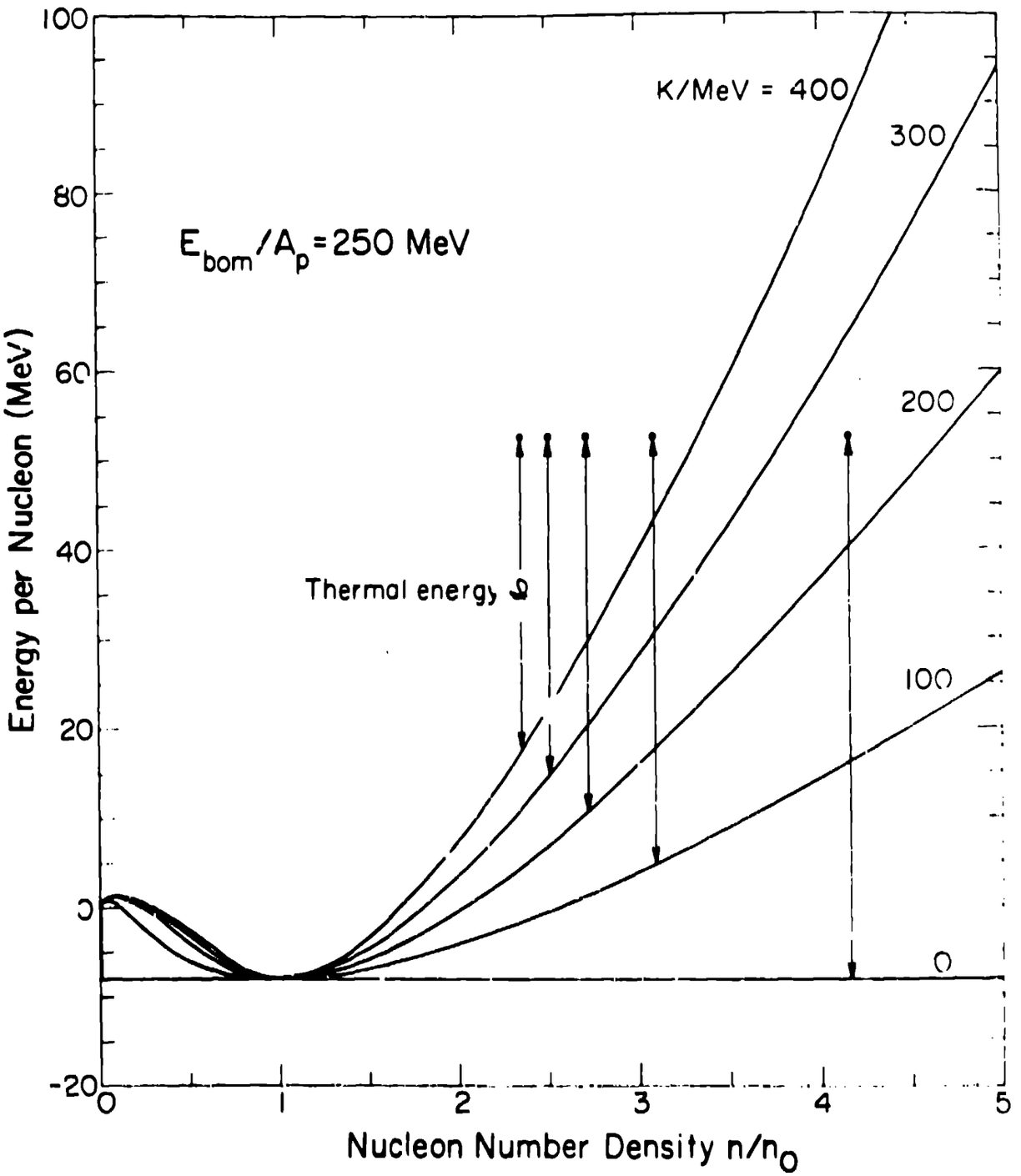
K/MeV = 400
300
200
100
0
$E_{bom}/A_p = 250$ MeV
Thermal energy
Energy per Nucleon (MeV)
Nucleon Number Density n/n_0
100
80
60
40
20
0
-20
0
1
2
3
4
5

Figure 1

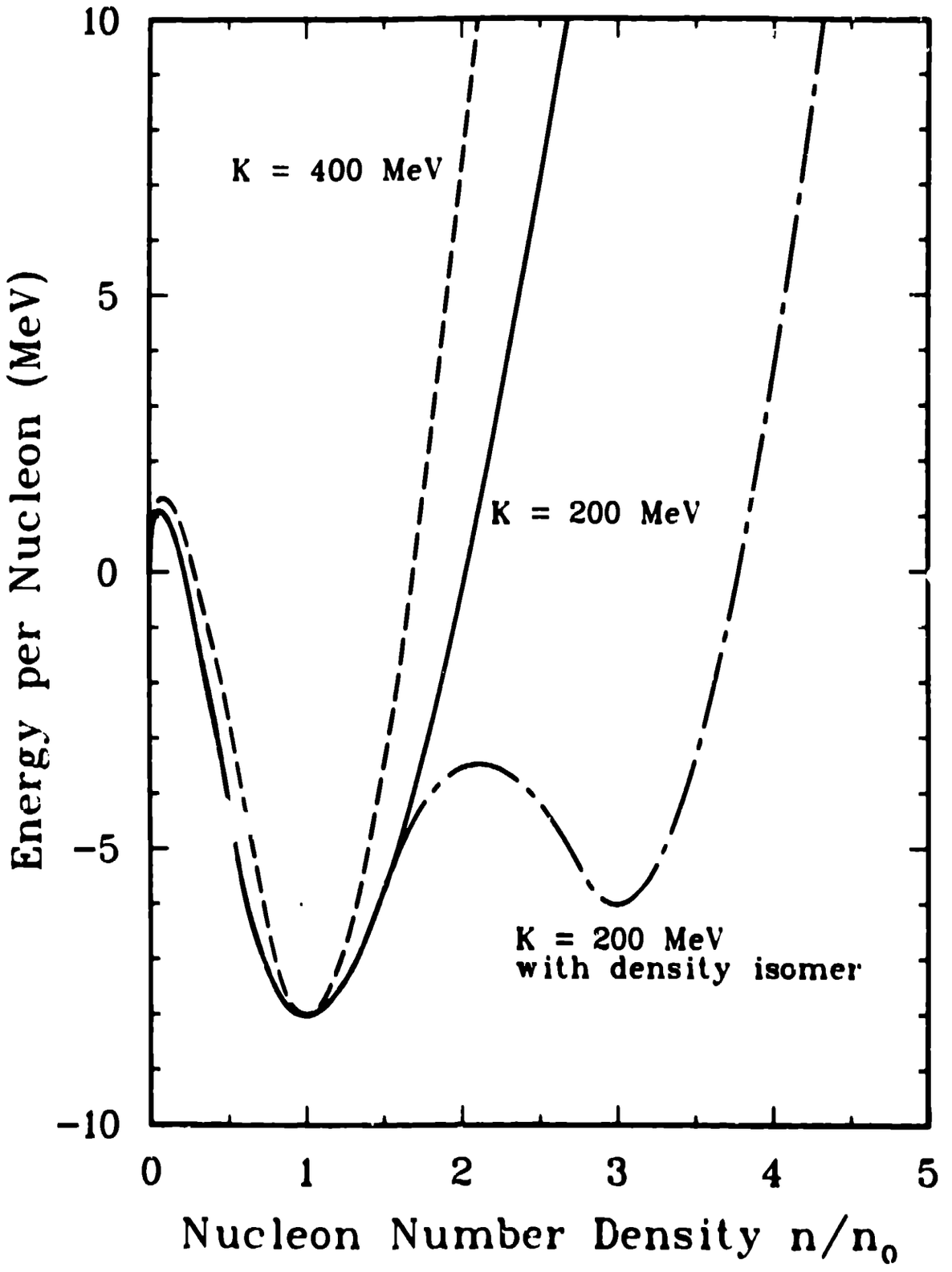
10
5
0
−5
−10
0
1
2
3
4
5
Energy per Nucleon (MeV)
Nucleon Number Density n/n0
K = 400 MeV
K = 200 MeV
K = 200 MeV
with density isomer

Figure 2

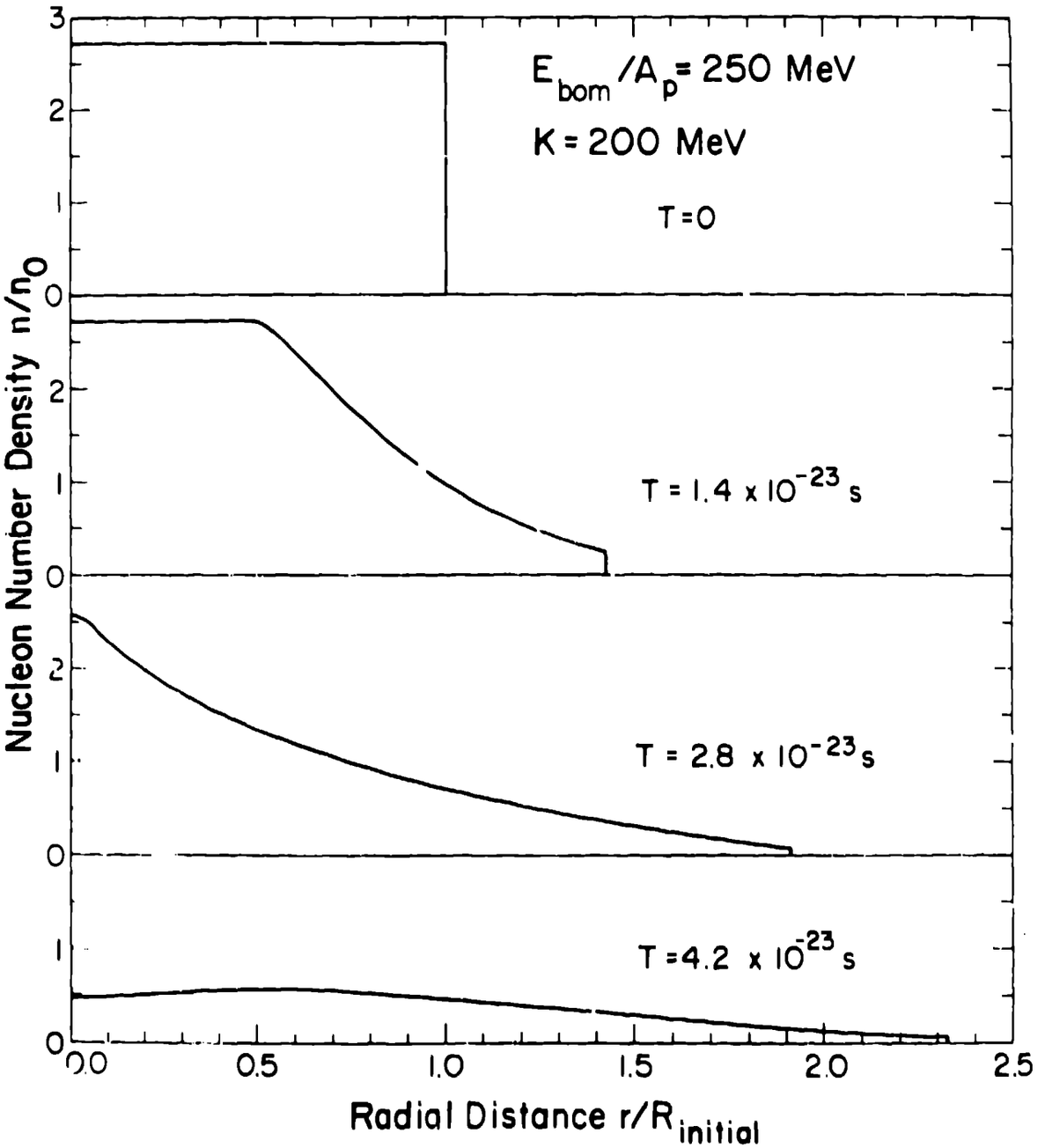
E_{bom}/A_p= 250 MeV
K = 200 MeV
T=0
T = 1.4 x 10^{-23} s
T = 2.8 x 10^{-23} s
T =4.2 x 10^{-23} s
Nucleon Number Density n/n_0
Radial Distance $r/R_{initial}$
0.0
0.5
1.0
1.5
2.0
2.5

Figure 3

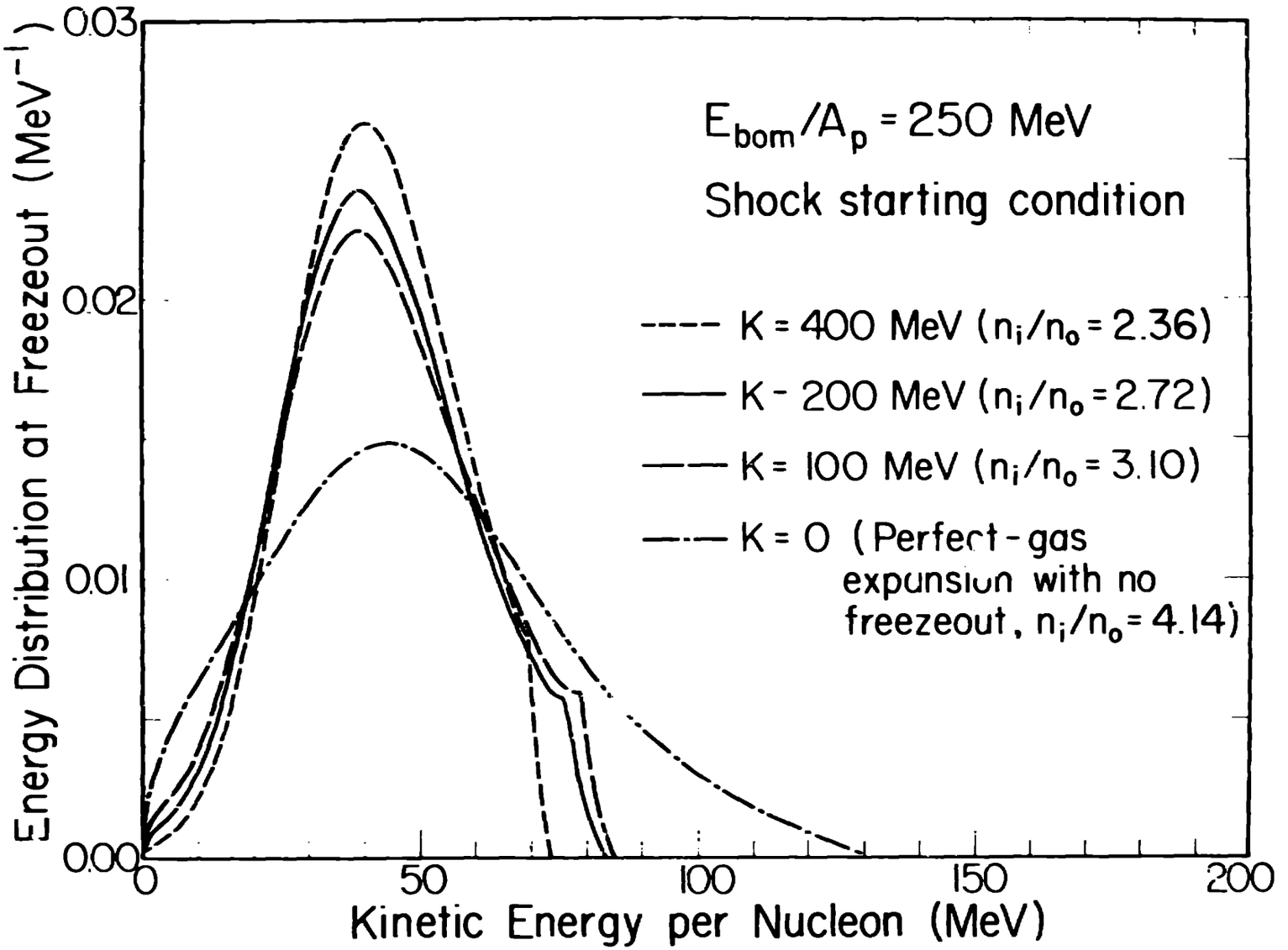
Energy Distribution at Freezeout (MeV⁻¹)
0.03
0.02
0.01
0.00
0
50
100
150
200
Kinetic Energy per Nucleon (MeV)
E_{bom}/A_p = 250 MeV
Shock starting condition
---- K = 400 MeV (n_i/n_o = 2.36)
—— K - 200 MeV (n_i/n_o = 2.72)
—— K = 100 MeV (n_i/n_o = 3.10)
—·— K = 0 (Perfect-gas expansion with no freezeout, n_i/n_o = 4.14)

Figure 4

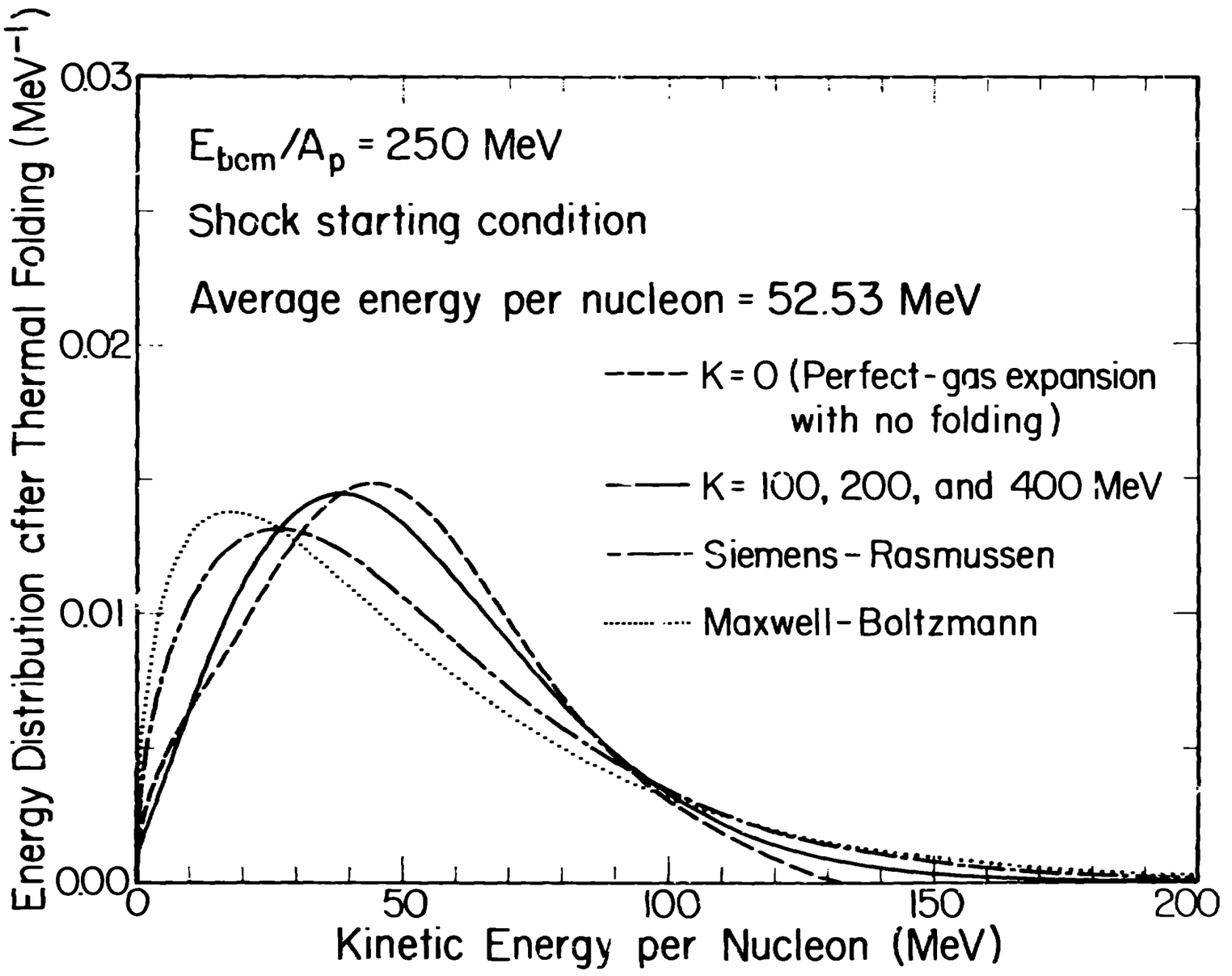
Energy Distribution after Thermal Folding (MeV⁻¹)
0.03
0.02
0.01
0.00
E_{bcm}/A_p = 250 MeV
Shock starting condition
Average energy per nucleon = 52.53 MeV
K = 0 (Perfect-gas expansion with no folding)
K = 100, 200, and 400 MeV
Siemens-Rasmussen
Maxwell-Boltzmann
0
50
100
150
200
Kinetic Energy per Nucleon (MeV)

Figure 5

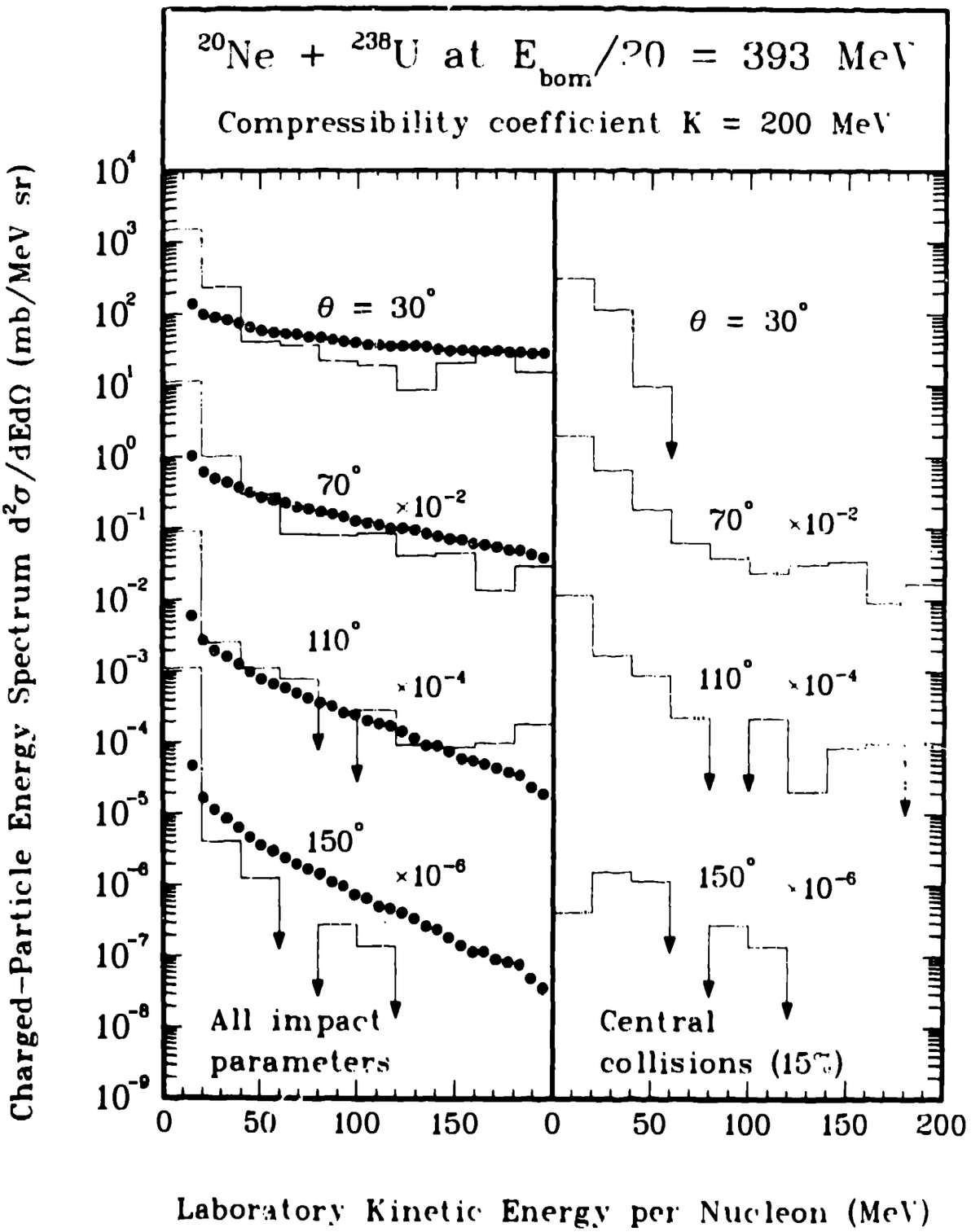
$^{20}Ne + ^{238}U$ at $E_{bom}/20 = 393$ MeV
Compressibility coefficient K = 200 MeV
Charged-Particle Energy Spectrum $d^2\sigma/dEd\Omega$ (mb/MeV sr)
θ = 30°
70°
$\times 10^{-2}$
110°
$\times 10^{-4}$
150°
$\times 10^{-6}$
All impact parameters
Central collisions (15%)
Laboratory Kinetic Energy per Nucleon (MeV)

Figure 6

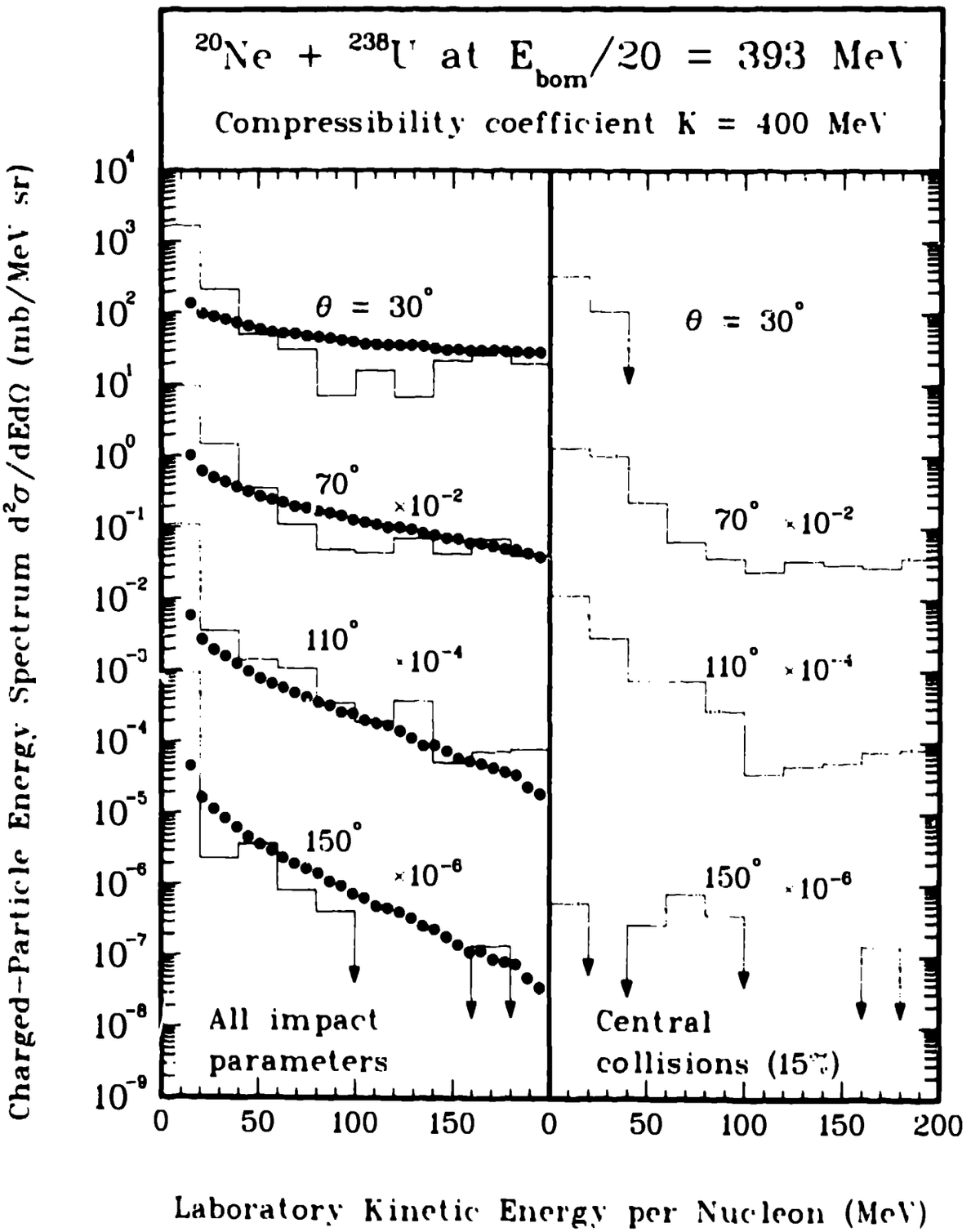
$^{20}Ne + ^{238}U$ at $E_{bom}/20$ = 393 MeV
Compressibility coefficient K = 400 MeV
Charged-Particle Energy Spectrum $d^2\sigma/dEd\Omega$ (mb/MeV sr)
θ = 30°
70°
$\times 10^{-2}$
110°
$\times 10^{-4}$
150°
$\times 10^{-6}$
All impact parameters
Central collisions (15%)
Laboratory Kinetic Energy per Nucleon (MeV)

Figure 7

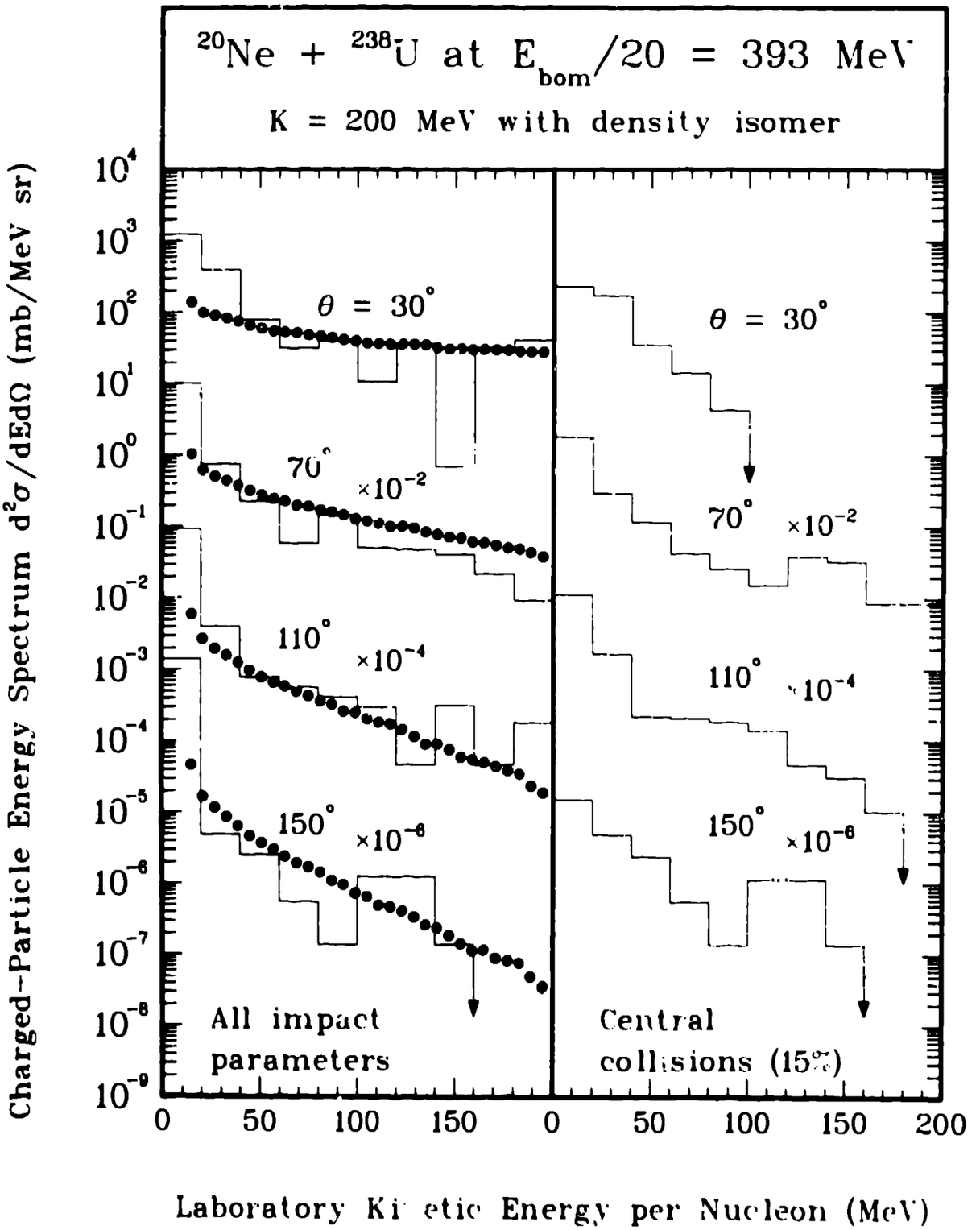
$^{20}Ne + ^{238}U$ at $E_{bom}/20$ = 393 MeV
K = 200 MeV with density isomer
Charged-Particle Energy Spectrum $d^2\sigma/dEd\Omega$ (mb/MeV sr)
θ = 30°
70°
×10⁻²
110°
×10⁻⁴
150°
×10⁻⁶
All impact parameters
Central collisions (15%)
Laboratory Kinetic Energy per Nucleon (MeV)

Figure 8